J. Fluid Mech. (1980), *vol.* 97, *part* 3, *pp.* 591–621
Printed in Great Britain

The propulsion by large amplitude waves of uniflagellar micro-organisms of finite length

By R. D. DRESDNER,† D. F. KATZ‡ AND S. A. BERGER
Department of Mechanical Engineering, University of California, Berkeley 94720

(Received 26 June 1978 and in revised form 28 August 1979)

The fluid mechanics of self-propelling, slender uniflagellar micro-organisms is examined theoretically. The mathematical analysis of these motions is based upon the Stokes equations, and the body is represented by a continuous distribution of stokeslets and doublets of undetermined strength. Since the body is self-propelling, additional constraints on the total force and moment upon it are applied. A system of singular integral and auxiliary equations, in which the propulsive velocity and viscous force per unit length are the unknowns, is derived. The vector integral equation is decomposed into near- and far-field contributions, and the solution is determined by a straightforward iterative procedure. The flagella considered are of constant radius and are restricted to planar undulations. The analysis is applied to a small amplitude wave form of infinite length, and a third-order analytic solution is obtained. By means of numerical computation, the method is extended to large amplitude wave forms of both infinite and finite length. The validity and accuracy of the solution method, the effect of local curvature, and an approximate model for an attached cell body-proper are evaluated in light of alternative theories.

The solution method is systematically applied to a variety of wave-form shapes representative of actual flagella. For a sinusoidal wave form, the variations in propulsive velocity, power output and propulsive efficiency are examined as functions of the number of wavelengths on the flagellum, the amplitude and the flagellar radius. Wave forms of variable amplitude and variable wavelength are also considered. Among the significant results are the effect of the cell body on pitching, the significant differences between constant frequency and constant phase-speed undulations for variable wavelength wave forms, and comparisons with other pertinent theories.

1. Introduction

Mathematical description of the hydrodynamics of swimming uniflagellar micro-organisms began with Taylor (1951), who modelled the body surface as an infinite two-dimensional sheet. Shortly thereafter, Taylor (1952) and Hancock (1953) considered a more realistic morphological model, in which the body consisted of a circular cylinder of very large aspect ratio. Hancock's analysis contains two features of particular importance. In defining a fundamental singularity, or stokeslet, as a solution to the Stokes equations, he helped lay the groundwork for contemporary slender-body theory

† Present address: Bioengineering Program, University of Illinois at Chicago Circle, Chicago, IL 60680.

‡ Also Department of Obstetrics and Gynecology, School of Medicine, University of California, Davis, CA 95616.

0022–1120/80/4422–8860 $02.00

at low Reynolds number. Moreover, he considered a body whose surface undulations consist of travelling waves of finite amplitude in comparison to wavelength. Such finite-amplitude undulations are characteristic of a great majority of uniflagellar micro-organisms, including bacteria, protozoa and spermatozoa. Hancock's method employs a distribution of stokeslets and potential doublets along the centre-line of a flagellum of effectively infinite length, in a manner analogous to slender airfoil theory. Solution of the governing integral equations was performed by Fourier analysis. Based on Hancock's earlier analysis Gray & Hancock (1955) introduced a simplified, approximate method, intended for widespread practical use. In their method, subsequently referred to as resistive force theory, hydrodynamic interactions between neighbouring elements of a flagellum are neglected. A constant tensorial relationship links local forces on a flagellar cross-section to the absolute velocity of that cross-section. The cell body-proper or head of the organism was analogously treated by Gray & Hancock as an isolated sphere. Since intraflagellar interactions are neglected, resistive force theory is thus only strictly valid in the limit of infinitely thin flagella. Nonetheless, this approach has received broad application during the past 20 years (e.g. Chwang & Wu 1971; Holwill & Miles 1971; Brokaw 1970; Pironneau & Katz 1974). Notably, it was in the application of resistive force theory that the proper balancing of longitudinal moments on a finite organism was formulated (Brokaw 1970). Improved expressions for the coefficients of the resistive force tensor have been developed by Lighthill (1975, 1976). His analyses were also based upon distribution of singularities along the centre-line of the flagellum, and account was taken of intraflagellar hydrodynamic interactions.

Other approaches have also been developed for the flagellar swimming problem. Recently Johnson (1977) has introduced higher-order singularities to the centre-line distribution to more accurately include the effects of local curvature. Johnson, however, did not consider a free-swimming body, but rather the force distribution due to an arbitrary unidirectional translation of the organism. A technique formulated by Cox (1970) for rigid slender bodies has been applied to flagella undergoing finite-amplitude undulations (Shen *et al.* 1975; Keller & Rubinow 1976). This approach analyses the flow field about the body by the method of matched asymptotic expansions, as developed in ascending powers of the reciprocal of the logarithm of an effective aspect ratio. The lowest-order application of Cox's method (see Keller & Rubinow 1976) does not include interaction between neighbouring flagellar elements, and consequently amounts to the resistive force approximation. The first-order application (Shen *et al.* 1975) does include such interaction. Finally, in an altogether different approach, a helical flagellum has been treated as an array of contiguous spherical beads (Garcia de la Torre & Bloomfield 1977). The fluid velocity field is obtained as a function of the forces acting at each bead through Oseen-type hydrodynamic interaction tensors.

Despite these many diversified studies during the past 28 years, certain fundamental issues in the theory of flagellar hydrodynamics remain to be investigated. In particular, no direct treatment has yet been given for a freely-swimming flagellum of finite length propagating planar waves of finite amplitude. Such a treatment properly should allow for propulsive motions with three degrees of freedom, two in translation and one in rotation. Hydrodynamic interactions between neighbouring flagellar segments must be taken into account. An inert head at one end of the flagellum is involved in such

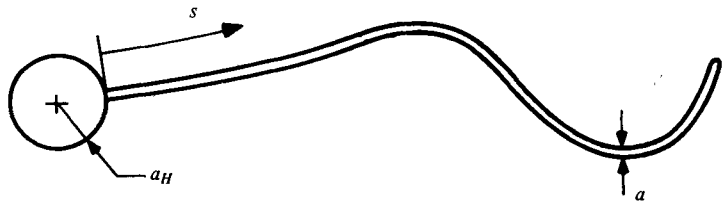

FIGURE 1. Schematic drawing of a uniflagellar micro-organism.

interactions and influences the propulsive velocities in all three degrees of freedom. The present study focuses upon these as yet incompletely addressed issues.

While perhaps not as conceptually simple as resistive force theory, the analysis presented here is designed to be more accurate, versatile, and not overburdened with extensive numerical calculations. The slender body of the organism is modelled by a continuous line distribution of singularities of unknown strength. A governing system of equations, based upon the integral equation derived by Hancock (1953) and the dynamical constraints introduced by Brokaw (1970) is formulated. The integral equation involving the unknown propulsive velocity and force distribution is decomposed into near- and far-field components, and the solution is obtained by an iterative procedure. The validity of the model is then tested by comparing solutions derived from it with those from existing theories. It is also shown how the interactive effect of a cell body attached to the flagellum may be included in the model.

Although several theories have been proposed to describe the fluid mechanical motion of the micro-organisms under consideration, none has been extensively applied to the numerous situations of biological interest. Thus, one of the primary objectives of this study is to systematically exercise the model developed here as a 'tool' to investigate a wide range of cases.

2. Theoretical development

2.1. *General theory*

Consider an isolated, self-propelling slender body in an unbounded fluid. The flagellum of the organism is modelled as an axisymmetric deformable, but inextensible filament of length L and radius a, with $a \ll L$ (figure 1). The co-ordinate measured along the flagellum or 'tail' is denoted by s. A spherical cell body-proper of radius $a_H = O(a)$ may be attached to the proximal end of the organism ($s = 0$). In this model the time-dependent position and velocity along the body are given in a co-ordinate system moving with the organism. The objective of this analysis is to determine the time-varying velocity of this moving co-ordinate system with respect to the stationary fluid at infinity. This velocity is interpreted as the 'propulsive' velocity of the micro-organism. Additionally, the viscous force distribution along the body is sought along with various derived quantities such as the power output and bending moment distribution. Movements of the organism are confined to a plane, but the method presented here can easily be extended to allow for more general motions.

Since both the steady and unsteady (based on beat frequency) Reynolds numbers for the micro-organisms under consideration are of order 10^{-2} or less, the fluid mechanical analysis proceeds from the linear, inertialess Stokes equations. The

flagellum of the micro-organism is modelled as a continuous distribution of singularities placed along its centre-line. As in several other studies (e.g. Hancock 1953; Batchelor 1970; Blake 1972; Lighthill 1975) only the stokeslet and doublet singularities are included in this model. An isolated stokeslet or point force located by the position vector $\mathbf{r}'$ generates an induced velocity at the point $\mathbf{r}$ given by

$$u_j = \frac{F_i}{8\pi\mu}\left(\frac{\delta_{ij}}{R}+\frac{R_i R_j}{R^3}\right) \equiv F_i G_{ij} \quad (i,j = 1,2,3). \tag{2.1}$$

In this equation $\mathbf{R} = \mathbf{r}-\mathbf{r}'$ and $R = |\mathbf{r}-\mathbf{r}'|$, and both position vectors are with respect to some convenient co-ordinate system. The strength of the stokeslet is given by F_i; δ_{ij} is the Kronecker delta; μ is the absolute viscosity of the fluid; and G_{ij} is the Green's function of the stokeslet. Similarly, the velocity field of an isolated doublet is given by

$$u_j = \frac{D_i}{4\pi}\left(\frac{\delta_{ij}}{R^3}-\frac{3R_i R_j}{R^5}\right) \equiv D_i H_{ij} \quad (i,j = 1,2,3), \tag{2.2}$$

where D_i is the doublet strength and H_{ij} is its Green's function.

If the body is modelled as a continuous distribution of these singularities placed along its centre-line, the induced velocity on the surface of the organism is given by

$$\mathbf{u}(s) = \int_0^L [\mathbf{f}(s').\mathbf{G}(S,S')+\mathbf{d}(s').\mathbf{H}(s,s')]\,ds'. \tag{2.3}$$

In order to invert this equation for the unknown stokeslet and doublet strengths per unit length, $\mathbf{f}$ and $\mathbf{d}$ respectively, the absolute velocity of the surface $\mathbf{u}(s)$ must be specified. For a free swimming organism the absolute velocity of a point on the flagellum is not known *a priori*. Indeed the complete swimming problem requires that the propulsive velocity be determined simultaneously with the force distribution. This velocity results when the organism appropriately deforms its body shape in time, generally by passing periodic travelling waves down its tail in the opposite direction. The total, or absolute velocity, of a point s can be decomposed into a 'beat' velocity due to tail deformations and a propulsive velocity of the whole organism, i.e.

$$\mathbf{u}(s,t) = \hat{\mathbf{u}}(s,t)+\mathbf{U}_p(t), \tag{2.4}$$

where $\hat{\mathbf{u}}$ is the beat velocity and $\mathbf{U}_p$ is the propulsive velocity. The beat velocity will be a specified function with respect to a co-ordinate system moving with the organism: it is determined by taking a Lagrangian time derivative of the position vector. The propulsive velocity corresponds to the rigid body motion of the organism with respect to a fixed reference frame (i.e. the fluid at infinity); it is the velocity of the (moving) co-ordinate frame in which the beat velocity is specified. The axes of the fixed co-ordinate system will be denoted by X and Y and of the moving system by x and y (figure 2). For general planar motion, there are three components of propulsive velocity: two translational, U_{px} and U_{py}, and one angular, Ω; therefore the total velocity, from (2.4), can be written as

$$\mathbf{u}(s,t) = \hat{\mathbf{u}}(s,t)+U_{px}\mathbf{i}+U_{py}\mathbf{j}+\Omega\mathbf{k}\wedge\mathbf{r}(s,t). \tag{2.5}$$

Here $\mathbf{i}$, $\mathbf{j}$, and $\mathbf{k}$ are unit vectors parallel to the x, y, and z axes, respectively.

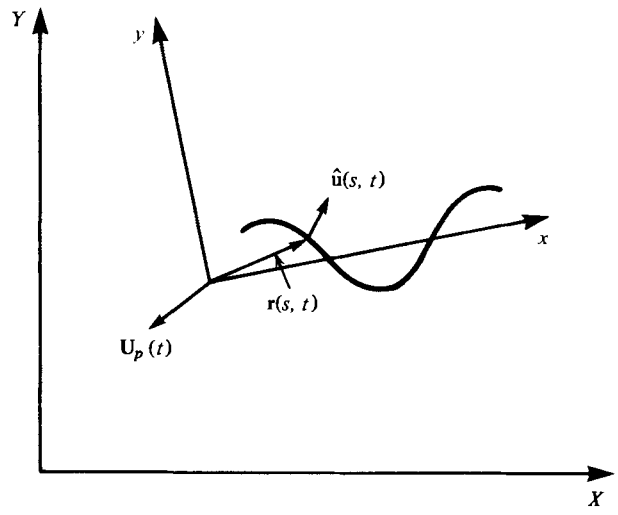

FIGURE 2. The X, Y co-ordinate system is a fixed reference frame. The local, moving co-ordinate system is denoted by x, y. The local system moves relative to the X, Y system with propulsive velocity $\mathbf{U}_p(t)$. In the x, y system, a point on the tail s has position $\mathbf{r}(s, t)$ and velocity $\hat{\mathbf{u}}(s, t)$.

In this study two different moving co-ordinate system representations are considered. The first co-ordinate system is applicable to wave forms of the type $y = y(x, t)$, but here its use is limited to sinusoidal shapes given by

$$y = b \sin k(x - ct), \tag{2.6}$$

where b is the amplitude, k the wavenumber and c the phase speed. The system in which this representation is applied will be referred to as the mean co-ordinate system, since the Lagrangian beat velocity is determined with respect to the mean position, (over a beat cycle) of the point $s = 0$. In the second moving system, the wave form is characterized by the slope angle of the local tangent to the flagellum, α, which is a function of the co-ordinates s and t, i.e.

$$\alpha = \alpha(s, t). \tag{2.7}$$

This wave-form specification, employed in conjunction with what will be referred to as the head co-ordinate system, will be used to model wave forms of more general shape than the mean system representation. Expressions for $\hat{\mathbf{u}}$ in both systems and further details can be found in the appendix.

Inserting (2.5) into the left-hand side of (2.3) increases the number of unknowns by the three scalar components of propulsive velocity. This necessitates that an equal number of supplementary equations be supplied. These can be obtained by considering the dynamics of the body itself in addition to the dynamics of the fluid. Applying Newton's second law of motion, and neglecting accelerations, constraints on the total force and moment $\mathbf{M}$ on the body reduce to

$$\int_0^L \mathbf{f}\, ds' = 0, \tag{2.8a}$$

$$\int_0^L \mathbf{r} \wedge \mathbf{f}\, ds' \equiv \int_0^L \mathbf{M}\, ds' = 0. \tag{2.8b}$$

These auxilliary equations will be referred to as the equilibrium conditions. Equations (2.3) and (2.8) are the coupled system that determines the propulsive velocity and force distribution.

Before proceeding to the next section, two of the assumptions of the analysis, one explicit and one implicit, are worthy of note. Since the body is slender it might be anticipated that the solution obtained by a line distribution of singularities would not differ substantially from that obtained from a surface distribution. (This latter representation can be shown to provide the exact solution; see Ladyzhenskaya 1969.) However, this is strictly true only in the case of an infinite straight slender body, or one for which the local axial curvature varies only slightly. This is not the case for real micro-organisms for which the curvature can be of $O(L)$ or larger. As will be shown in § 3, however, the present model does not sacrifice any significant accuracy by including such an assumption. The effect of the body tips, located as $s = 0$ and $s = L$, while of interest (see, e.g., Tuck 1964, Tillett 1970; Johnson 1977), has not been included in this study. Since the singularities (extending from $s = 0$ to $s = L$) must be internal to the body, the actual body length is slightly longer than L and the precise tip shape is undetermined. The work of Johnson (1977) indicates that the tip effect is at most of the same order as other simplifications inherent in this analysis.

2.2. *Decomposition of the integral equation and solution method*

Since the body under consideration is slender, a reasonable simplification of (2.3) is to apply the velocity boundary condition on the body centre-line rather than on the body surface. However, the integral equation then becomes singular when $\mathbf{r} = \mathbf{r}'$. This difficulty can be circumvented, and the advantages of slender body theory still retained, if (2.3) is decomposed into two parts as follows:

$$\mathbf{u}(s) = \int_{s-\delta(s)}^{s+\delta(s)} [\mathbf{f}(s').\mathbf{G}(s,s') + \mathbf{d}(s').\mathbf{H}(s,s')]\,ds' + \int_{0}^{s-\delta(s)} + \int_{s+\delta(s)}^{L} [\mathbf{f}(s').\mathbf{G}(s,s') + \mathbf{d}(s').\mathbf{H}(s,s')]\,ds'. \tag{2.9}$$

The function $\delta(s)$, as yet an unspecified parameter, is assumed to lie in the range

$$a \ll \delta(s) \ll \Lambda, \tag{2.10}$$

where Λ is a measure of the distance along which the shape of organism has spacial periodicity (e.g., the wavelength measured along s).

The integral constituting the first term in (2.9) contributes a 'local' effect to the total velocity of a given point on the body. Within this near-field region, $\mathbf{r} \simeq \mathbf{r}'$, and the velocity boundary condition is evaluated on the body surface, thereby avoiding the singularity. It is assumed that within the limits of this integral, i.e. $s-\delta \leqslant s' \leqslant s+\delta$, the singularity strengths are constant. The details involved in this assumption can be found in Hancock (1953, see, e.g., § 2), and its justification will be demonstrated *a posteriori* in § 3. It follows that the velocity boundary condition need only be applied on a single cross-section of the body within the near-field region (centred at $\mathbf{r} = \mathbf{r}'$). In summary, the near-field contribution to $\mathbf{u}$ on the body surface is due to a straight line distribution of stokeslets and doublets.

The second term in (2.9) represents the far-field effect of singularities outside the

region encompassed by the first integral. Here the simplification is made that since the far-field doublet contribution to the velocity at a point on the surface is of higher order than the stokeslet contribution, it can be neglected (for details see Hancock 1953, or Lighthill 1975). In addition, equation (2.10) and the slenderness criterion allow the far-field induced velocity contribution to be applied to the body centreline rather than the body surface, with an error of $O(a^2/\delta^2)$. These simplifications greatly reduce the computational effort in evaluating the far-field contribution.

In light of the above, (2.9) can be written as

$$\mathbf{u}(s) = \mathbf{f}(s).\int_{s-\delta(s)}^{s+\delta(s)} \mathbf{G}(s,s')\,ds' + \mathbf{d}(s).\int_{s-\delta(s)}^{s+\delta(s)} \mathbf{H}(s,s')\,ds' + \int_0^{s-\delta(s)} + \int_{s+\delta(s)}^{L} \mathbf{f}(s').\mathbf{G}(s,s')\,ds'. \tag{2.11}$$

The function $\delta(s)$ now is assumed to have a constant value. Since the final results are found to be relatively independent of the exact choice of δ, as specified within the range given by (2.10), this simplification appears to be justified (see § 3).

It remains to evaluate the integrals of the tensors $\mathbf{G}$ and $\mathbf{H}$. In effect, the near-field contribution is that of a slowly translating, right circular cylinder of radius a and finite length 2δ. The cogent analysis of Lighthill (1975) concerning this problem may be readily applied. The motion is first resolved into normal and longitudinal movement of the cylinder. For normal translation, in order to satisfy the no-slip velocity boundary condition on the central cross-section, both normal stokeslets and doublets are necessary. In addition, the normal doublet strength per unit length is given in terms of the normal stokeslet strength per unit length as $d_N = f_N a^2/4\mu$. In contrast, for longitudinal motion no doublets are needed to match the velocity boundary condition.

In terms of local normal and longitudinal components, the near-field contribution to $\mathbf{u}$ can then be written as

$$u_N = f_N/C_N, \quad u_L = f_L/C_L, \tag{2.12}$$

where

$$C_N = 8\pi\mu/[\ln(\beta_1+1)/(\beta_1-1) + 2/\beta_1\beta_2], \tag{2.13a}$$

$$C_L = 4\pi\mu/[\ln(\beta_1+1)/(\beta_1-1) - 1/\beta_1]. \tag{2.13b}$$

Here $\beta_1 = (1+a^2/\delta^2)^{\frac{1}{2}}$ and $\beta_2 = 2+a^2/\delta^2\beta_1^2$. Applying (2.10) to (2.13) and dropping terms of $O(a^2/\delta^2)$ gives

$$C_N = 4\pi\mu/[\ln(2\delta/a) + 0{\cdot}5], \tag{2.14a}$$

$$C_L = 2\pi\mu/[\ln(2\delta/a) - 0{\cdot}5]. \tag{2.14b}$$

Equation (2.12) shows that the near-field velocity contribution is linearly proportional to the local force or stokeslet strength per unit length. The constants (for a given body) C_N and C_L, the so-called 'resistance' or 'force coefficients', form the basis of the low-Reynolds-number resistive force theory initiated by Gray & Hancock (1955).† We note that the use of resistance coefficients is only a 'zeroth-order' approximation for all but the most elementary bodies.

We now consider the effect of an attached cell body. The no-slip velocity boundary

† Gray & Hancock (1955) assumed that $C_N = 2C_L$ and that a non-interacting spherical cell body-proper was present. They then obtained an expression for C_L analogous to (2.14*b*) but with $\delta = O(\Lambda)$.

condition must be satisfied on the head surface as well as on the tail. The organisms under consideration here have heads with an average radius a_H (based on head volume and a spherical model) ranging up to approximately $L/30$. (Human sperm, for example, have an a_H/L ratio of about 1/40; see Katz & Pedrotti (1977).) In the following analysis the shape will be approximated as a sphere; but even with this simplification, since the flow due to a moving sphere in the presence of arbitrary boundaries (e.g., the body tail) is extremely complex, the problem will be solved approximately.

As is well known, the motion of an isolated sphere can be represented by a single stokeslet and doublet at the centre of the body. The force and moment on the head, $\mathbf{F}_H$ and $\mathbf{M}_H$ respectively, can be written in terms of its absolute translational velocity $\mathbf{u}_H$ and angular velocity $\boldsymbol{\Omega}_H$ as (Happel & Brenner 1973)

$$\mathbf{F}_H = -C_H \mathbf{u}_H, \quad \mathbf{M}_H = -C_M \boldsymbol{\Omega}_H + \mathbf{r}_H \wedge \mathbf{F}_H, \tag{2.15}$$

where $C_H = 6\pi\mu a$ and $C_M' = 8\pi\mu a^3$. The constants C_H and C_M can be thought of as resistance coefficients. The vector $\mathbf{r}_H$ is the position of the centre of the sphere with respect to the point about which the moment is taken. Since the total velocity of the organism is unknown, the head will be represented by a stokeslet–doublet pair of unknown strength. The velocity at a point on the surface of the spherical head is composed of two contributions: a near-field effect, given by (2.15), and a far-field velocity due to the stokeslets distributed along the tail. Similarily the far-field velocity at a point on the tail includes an additional component due to the head. Thus we allow for higher-order interactions between the cell body and the tail. The critical assumption is then made that the velocity on the head is evaluated at the sphere's centre rather than on its surface. This slender-body-type simplification is not strictly valid for stokeslets distributed along roughly the proximal 10 % of the tail. In this range of s the distance from a point on the flagellum to the head centre may differ significantly from that to a point on the head surface. The result of the simplifications noted above is that the head is effectively treated as an additional tail segment with resistance coefficients given by C_H and C_M. In the following section, the validity of the modelling procedure for the head will be examined.

For a self-propelling body with a cell body the total velocity given by (2.11) must be modified to account for the mutual interactive effect of the head and tail. Furthermore, the force and moment on the head, given by (2.15), must be added to the left-hand sides of the equilibrium conditions (equations (2.8*a*) and (2.8*b*), respectively). The head–tail junction is assumed to be rigid. Thus the total angular velocity of the head is $\boldsymbol{\Omega}_H = [\Omega + (\partial\alpha/\partial t)\,(s = 0, t)]\,\mathbf{k}$, and the position vector to the head centre is

$$\mathbf{r}_H = [x(s = 0, t) - a_H \cos\alpha(s = 0, t)]\,\mathbf{i} + [y(s = 0, t) - a_H \sin\alpha(s = 0, t)]\,\mathbf{j}. \tag{2.16}$$

Combining (2.5), (2.8), (2.11), (2.15) and the above, the complete system of equations for the motion of the organism is

$$\mathbf{u}(s, t) = \hat{\mathbf{u}}(s, t) + \mathbf{U}_p(t) = \mathbf{f}(s, t) \,.\, \mathbf{C}^{-1} + \int_0^{s-\delta} + \int_{s+\delta}^{L} \mathbf{f}(s', t) \,.\, \mathbf{G}(s, t; s', t)\, ds', \tag{2.17a}$$

† For a flagellum with a head, the total velocity at a point on the tail includes the additional term $[\mathbf{G} + (a_H^2/6\mu)\,\mathbf{H}] \,.\, \mathbf{F}_H$. Moreover, the total velocity of the head is given by

$$\mathbf{u}_H = \mathbf{F}_H/C_H + \int_0^L \mathbf{f}(s', t) \,.\, \mathbf{G}(s, t; s', t)\, ds'.$$

$$\int_0^L \mathbf{f}(s',t)\,ds' - \mathbf{F}_H = 0, \tag{2.17b}$$

$$\int_0^L \mathbf{M}(s',t)\,ds' - \mathbf{M}_H = 0. \tag{2.17c}$$

In equation (2.17*a*)

$$\mathbf{C}^{-1} = \int_{s-\delta}^{s+\delta} \mathbf{G}(S,t;\,s',t)\,ds' + \frac{a^2}{4\mu}\int_{s-\delta}^{s+\delta} \mathbf{H}(S,t;\,s',t)\,ds',$$

where we note that the second integral is proportional to **nn**. The tensor **nn** is the dyadic product of the normal (to the local body centre-line) unit vector **n** with itself, and $\mathbf{f}.\mathbf{nn} = (\mathbf{f}.\mathbf{n})\,\mathbf{n}$.

2.3. *Iterative solution method*

Equations (2.17) are essentially a Fredholm integral equation with auxiliary equations which must be satisfied simultaneously, and, with the exception of a few, quite restrictive cases, cannot be solved analytically. There are various standard methods for solving such systems. For example, Johnson (1977) chose a matrix inversion technique since the propulsive velocity was assumed to be unidirectional and was specified. In this study an iterative approach, similar to the standard method of successive approximations (e.g. Hildebrand 1965) is employed. Among the advantages of this solution procedure are its conceptual simplicity and accommodation to both analysis and numerical computations.

For convenience, the far-field velocity contribution is defined as

$$\tilde{\mathbf{u}}(s,t) = \int_0^{s-\delta} + \int_{s+\delta}^{L} \mathbf{f}(s,t).\mathbf{G}(s,t;\,s',t)\,ds'. \tag{2.18}$$

Then, for any time t, (2.17*a*) can be written

$$\hat{\mathbf{u}}(s) + \mathbf{U}_p = \mathbf{f}(s).\mathbf{C}^{-1} + \tilde{\mathbf{u}}(s), \tag{2.19}$$

so that

$$\mathbf{f}(s) = \mathbf{C}.[\hat{\mathbf{u}}(s) + \mathbf{U}_p - \tilde{\mathbf{u}}(s)]. \tag{2.20}$$

The iteration is initiated by solving for a 'zeroth-order' force distribution in terms of an unknown zeroth-order propulsive velocity, viz.

$$\mathbf{f}^{(0)}(s) = \mathbf{C}.[\hat{\mathbf{u}}(s) + \mathbf{U}_p^{(0)}], \tag{2.21}$$

where the superscript denotes the order of the iteration. The term $\tilde{\mathbf{u}}(s)$ is taken to be zero, i.e. only the near-field effect is considered at the zeroth-order level. Substitution of this equation into (2.17*b*) and (2.17*c*) results in the following system of equations

$$\mathbf{V}.\mathbf{U}_p^{(0)} = \mathbf{W}. \tag{2.22}$$

The terms in **V** involve integrals of known functions of **C** and the given wave form. Since $\mathbf{U}_p$ is independent of s, it factors out of the integrals of (2.17). The vector **W** is also known and is a function of $\hat{\mathbf{u}}(s)$, **C**, the given wave form and the head resistance coefficients. Solving (2.22) for $\mathbf{U}_p^{(0)}$, the zeroth-order force (stokeslet) distribution is determined by (2.21).

A first-order force distribution is now defined by the equation

$$\mathbf{f}^{(1)}(s) = \mathbf{C}.[\hat{\mathbf{u}}(s) + \mathbf{U}_p^{(1)} - \tilde{\mathbf{u}}^{(0)}(s)],$$

where

$$\tilde{\mathbf{u}}^{(0)}(s) = \int_0^{s-\delta} + \int_{s+\delta}^{L} \mathbf{f}^{(0)}(s') \cdot \mathbf{G}(s, s')\, ds'.$$

The equation for $\mathbf{f}^{(1)}(s)$ is substituted into the equilibrium conditions, resulting in an equation analogous to (2.22). This determines $\mathbf{U}_p^{(1)}$, and the procedure can be carried out to as many orders as desired.

3. Numerical analysis and verification procedure

In order to study the propulsive moments of flagellated organisms of finite length undergoing large-amplitude undulations, a computer program as been developed for the iterative solution procedure outlined in the previous section. That is, successive estimates of the total velocity of specific points along the flagellum were improved by updated far-field contributions and repeated application of the equilibrium equations. The program, which was run on a CDC 7600 digital computer, requires that the body shape, Lagrangian beat velocity, resistance coefficients, and value of δ be known. Integrations along the tail (i.e. with respect to s) are performed by a Simpson's rule approximation. It was found that roughly fifty, equally spaced points per wavelength are sufficient to insure an acceptable truncation error. For periodic wave forms the cycle is divided into sixteen equal time steps. Since the velocity field at a given time depends only upon instantaneous values of the organism's shape and velocity distribution, the only restriction on the incrementization of time is that it be small enough so that temporal averages are accurate. Convergence, based upon the criterion that the total velocity at all tail points change by less than one percent between two successive iterations, is achieved within approximately ten iterative cycles. For a tail of one wavelength, a complete beat cycle requires approximately 5 seconds of central processor time.

Prior to considering the general wave form problem, various tests were carried out in order to evaluate both the accuracy of the model and the validity of certain crucial assumptions. At the zeroth-order level the solution was checked by a calculation of the propulsive velocity of a small amplitude, finite length sinusoidal wave form, a problem solved analytically by Pironneau & Katz (1974) and Shack, Fray & Lardner (1974). For a non-dimensional amplitude of $bk = 0{\cdot}01$ (this parameter will be used throughout to characterize sinusoidal wave forms) the calculated results agreed with the theory to three significant figures. For further details see Dresdner (1978).

δ Dependence

For higher-order interactive calculations δ must be specified. It should be noted that this is a direct consequence of the particular decomposition of the governing integral equation and iterative solution technique discussed in § 2. A purely analytic approach would not result in dependence on a numerical parameter of this type. Heretofore the only restriction on δ has been that expressed by (2.10). That is, the body is slender, and δ must be at least an order of magnitude smaller than the local radius of curvature. Within these bounds the sensitivity of the numerical results to variations in δ must be determined. The longitudinal component of propulsive velocity generally has been used for this evaluation since it provides a concise means for overall assessment of the results.

To aid in this investigation the iterative procedure was performed analytically, to third-order, for a small amplitude sinusoidal wave form of infinite length. The unidirectional propulsive velocity was found to be

$$U^{(3)}_{pX}/cb^2k^2 = (1-C_N/C_L)/2 - \frac{C_N}{8\pi\mu}\left\{1+\frac{C_N}{4\pi\mu}(\gamma+\ln\delta)\right.$$
$$\left.\times\left[1+\frac{C_N}{4\pi\mu}(\gamma+\ln\delta)\right]\right\}[1-\gamma-\ln\delta-(1-C_N/C_L)(\gamma+\ln\delta)], \quad (3.1)$$

where $\gamma = 0{\cdot}577$ is Euler's constant and $bk \ll 1$.

According to (3.1) the zeroth-order theory (the first term) depends only upon the ratio of the resistance coefficients, while the higher-order contribution depends upon the magnitude of these coefficients and the parameter δ. Lighthill (1975), considering the same geometric assumptions employed in the derivation of (3.1) obtained the following expression for δ

$$\delta/\lambda = 0{\cdot}08937. \quad (3.2)$$

The argument upon which this result is based is somewhat heuristic. However, since this value satisfies the criterion of (2.10), if a/L is $O(0{\cdot}01)$, we have used it as a nominal value. It is of interest to note that if (3.2) is substituted into (3.1) the expression for $U^{(3)}_{pX}$ reduces to the expression derived by Hancock (1953), as well as an identical one, obtained from zeroth-order theory into which Lighthill's (1976) improved resistance coefficients have been inserted (see § 5).

The sensitivity of $U^{(3)}_{pX}$ to variations in δ was investigated by assuming two extreme values of δ/λ ($0{\cdot}05$ and $0{\cdot}15$) in (3.1). Between these two extremes the variation in $U^{(3)}_{pX}$ was less than 3 %. Therefore for a flagellum of infinite length undergoing small amplitude undulations, the propulsive velocity is essentially insensitive to a reasonable choice of the δ parameter. The computer program was also tested by using (3.1). For the nominal value of δ/λ the error between theory and computation was also less than 3 %. In these computations the infinitely long flagellum was approximated by a finite length sinusoid of twenty wavelengths. The unidirectional motion was obtained by constraining the propulsive motions to the x direction only. In order to diminish end effects the single equilibrium equation was integrated over the two central wavelengths rather than the complete body length.

The sensitivity of large amplitude wave forms to variations in δ was also determined. A finite length flagellum with a sinusoidal wave form of one wavelength ($n = 1$), $a/L = 0{\cdot}01$, and $bk = 1{\cdot}0$ was considered. The value of δ/Λ was varied from $0{\cdot}05$ to $0{\cdot}2$. This four-fold increase in the δ parameter produced variations in the time-averaged propulsive velocities in the fixed reference system ($\overline{U}_{pX}$ and $\overline{U}_{pY}$) of the order of 5 %. (For large amplitude undulations the proper scaling of δ is Λ rather than λ; see e.g. Lighthill 1976.) The fact that such an extreme variation in δ results in a variation in time-averaged calculated quantities that is almost two orders of magnitude smaller, indicates the relative insensitivity of the solution method to this parameter.

For large amplitude undulations the numerical calculations were compared with two prior analyses. Hancock (1953) derived the same integral equation as developed in this study. He approximated the force distribution with a truncated Fourier series so that the far-field integrals could be numerically integrated with greater ease. Few

	Propulsive velocity (U_{pX}/c)		
a/λ	Hancock (1953)	Shen *et al.* (1975)†	Present study
0·01	−0·20	−0·203 (−0·194), −0·200 (−0·187)	−0·180
0·02	−0·17	−0·189 (−0·180), −0·177 (−0·169)	−0·167

† The range of values is discussed in § 3.

TABLE 1. Large amplitude infinite length flagellum ($bk = 1$).

details and no information on the accuracy of the solution method were given. In the second analysis, Shen *et al.* (1975) extended the inert, slender body theory developed by Cox (1970), employing the method of matched asymptotic expansions, to an infinite, self-propelling flagellum. Comparison with these earlier results has been made for two sinusoidal wave forms with $bk = 1{\cdot}0$ and aspect ratios of $a/\lambda = 0{\cdot}01$ and $a/\lambda = 0{\cdot}02$ and is shown in table 1. For each radius there are four values of U_{pX} for Shen *et al.*, since their analysis resulted in two values for C_N/C_L of equal accuracy. Shen *et al.* approximated certain elliptic integrals [their equation (39)] in order to simplify their computations. The numbers in parentheses are the corresponding values that result when more accurate expressions for these integrals are employed. For the iterative solution method a value of 0·08937 for δ/Λ was used. (For $a/\lambda = 0{\cdot}01$, $\delta/\Lambda = 0{\cdot}05$ was also tested with no appreciable change in results.) The comparison for $a/\lambda = 0{\cdot}01$ shows a 10 % variance with Hancock and a range of from four to 12 % with Shen *et al.* The results for $a/\lambda = 0{\cdot}02$ exhibit only a 2 % difference with Hancock and between a 2 and 14 % variation with Shen *et al.* These comparative results show good correlations between the three solution methods. Moreover, since a reasonable variation in δ did not effect the results, the Lighthill value of 0·08937 appears to be an adequate estimate (until a more precise value or s dependence is determined) for large amplitude wave forms.

Local curvature effects

The assumption that local curvature effects are small permitted the near-field contribution to be modelled by a straight, circular cylinder. To test the validity of this assumption, comparison with accurate results for a curved slender body is necessary. As a basis for evaluation a torus was chosen, with radius equal to the minimum local radius of curvature on a sine wave with $bk = 1{\cdot}0$ and $a/\lambda = 0{\cdot}01$. Resistance coefficients and the total force were calculated, via the computer program, for such a torus translating in a direction perpendicular to its longitudinal axis. Although the exact solution to this problem is not yet available, Johnson (1977) developed formulae for these quantities which are valid, to order $(a/L)^2$, in the range of curvature typically displayed by flagella. The comparison showed that the normal resistance coefficient C_N varied by less than 5 %, while C_L, C_N/C_L, and the total drag on the torus differed by less than three per cent. The variance in these quantities is judged to be quite acceptable, especially since the radius of curvature considered is an extreme value for flagella.

Head effect

To test the accuracy of the approximate head analysis presented in § 2, the special case of axisymmetric Stokes flow about a sphere attached to a straight slender body (de Mestre & Katz 1974) was employed. For this problem the total drag on the body and the singularity distribution along the slender tail are readily obtained by the method of images. The approximate representation described here was compared to the theoretical results of de Mestre & Katz for a body with $a_H/L = 1/36$ and $a/L = 0{\cdot}01$. The drag on the total body was calculated and found to underestimate the theoretical value by less than 6 %. The force distribution on the tail was qualitatively very similar to that shown in figure 5 of de Mestre & Katz. (The distribution very near the sphere, however, showed considerable variance due to the velocity boundary-condition simplification discussed in § 2.) If the sphere and tail are considered as non-interacting bodies, the combined drag on the body is given by the sum of the separate drag contributions. In this case the sphere drag is given by (2.15) and the tail drag may be found from (7.10) and (7.12*a*) of Cox (1970). For the body under consideration the total drag of the non-interacting head-tail system overestimates the theoretical result by slightly over 10 %. Inasmuch as an exact theory for the general case is highly complex, and since the approximate head effect method is both easy to apply and considerably more accurate than the non-interacting model, the technique presented here has been incorporated into the solution procedure.

4. Results and discussion

The fluid mechanical model presented in § 2 has been applied to essentially two types of studies. The first group was concerned with the systematic variation of wave-form parameters of an archetypal micro-organism. This 'archetype' consisted of a headless, sinusoidal travelling wave with $bk = 1$, one wavelength ($n = 1$), and aspect ratio (a/L) of 0·01. Such a configuration was chosen for both its conceptual simplicity and its approximate physiological and morphological attributes; it does not necessarily represent any particular organism or cell. Importantly, comparison with alternative theories was facilitated by this choice. The second group of studies involved the self-propulsion of flagellar shapes which are more physiologically accurate. These wave forms are characterized by an aperiodic amplitude envelope, and in some instances an s-dependent wavelength.

Since the propulsive velocity is determined in the local co-ordinate system, the absolute propulsive velocity of the organism is determined by resolving the translational components of $\mathbf{U}_p$ into the fixed co-ordinate system; thus

$$U_{pX} = U_{px}\cos\theta - U_{py}\sin\theta,$$
$$U_{pY} = U_{px}\sin\theta + U_{py}\cos\theta.$$

In the expression above θ, the pitching angle, is given by

$$\theta(t) = \int_0^t \Omega(t')\,dt' \quad (\theta(0) \equiv 0).$$

When the mean system representation is employed quantities are non-dimensionalized by c, μ, and λ (or k). These parameters are chosen for convenience and for purposes of

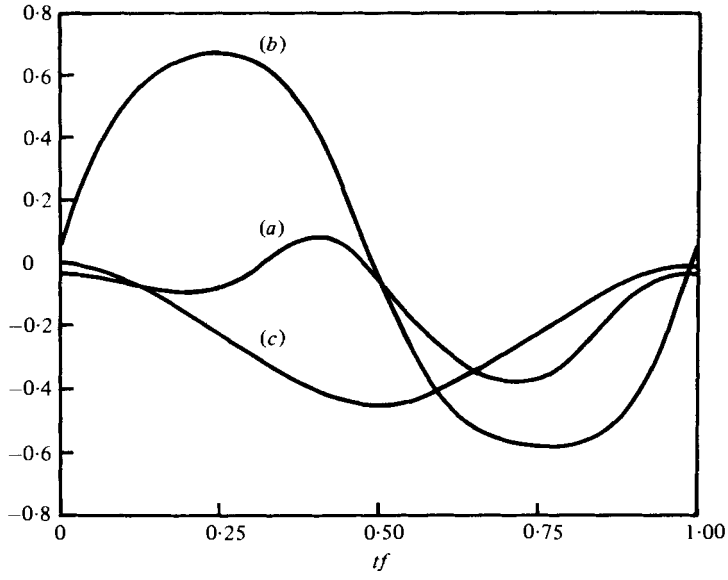

FIGURE 3. Temporal variation of (a) U_{pX}/c, (b) U_{pY}/c and (c) θ for a headless flagellum of shape given by $y = b \sin k(x-ct)$ with $bk = 1$, $n = 1$ and $a/L = 0{\cdot}01$ over a beat cycle.

comparison with other theories. In the head co-ordinate system, with its s-dependent α-generated wave, the length scale is more suitably taken as L. From an experimental point of view, the beat frequency f is usually easier to obtain than c, suggesting an alternative velocity scale, fL.† Inasmuch as different non-dimensionalizations may be more appropriate for different experimental circumstances, various non-dimensionalizations have been utilized.

In addition to the propulsive velocity and force distribution, other quantities are of interest. Among these are the rate of external hydro-mechanical energy production or power expended by the micro-organism in propelling itself through the fluid ($\dot{E}$), given by

$$\dot{E} = \int_0^L \mathbf{f}(s') \cdot \mathbf{u}(s')\, ds' + \mathbf{F}_H \cdot \mathbf{u}_H + \mathbf{M}_H \cdot \boldsymbol{\Omega}_H,$$

and the local bending moment with respect to the point $s = 0$ ($\mathbf{M}_B$), given by

$$\mathbf{M}_B(s) = -\int_0^s [\mathbf{r}(s') - \mathbf{r}(s)] \wedge \mathbf{f}(s')\, ds' + \mathbf{M}_H.$$

Effective resistance coefficients at a point on the body have been defined for normal (C'_N) and longitudinal (C'_L) translation. These are the ratio of a component of the force per unit length to its corresponding component of the total velocity, both taken at the final iteration. Also of interest is a cycle-averaged dimensionless propulsive efficiency for the organism. Traditionally, this has been defined in a form analogous to

$$\eta = \mu L \overline{U}_{pX}^2 / \overline{\dot{E}}, \tag{4.1a}$$

† To conform with standard use, the symbol f denotes frequency while the symbol $\mathbf{f}$ denotes the viscous force per unit length on the fluid.

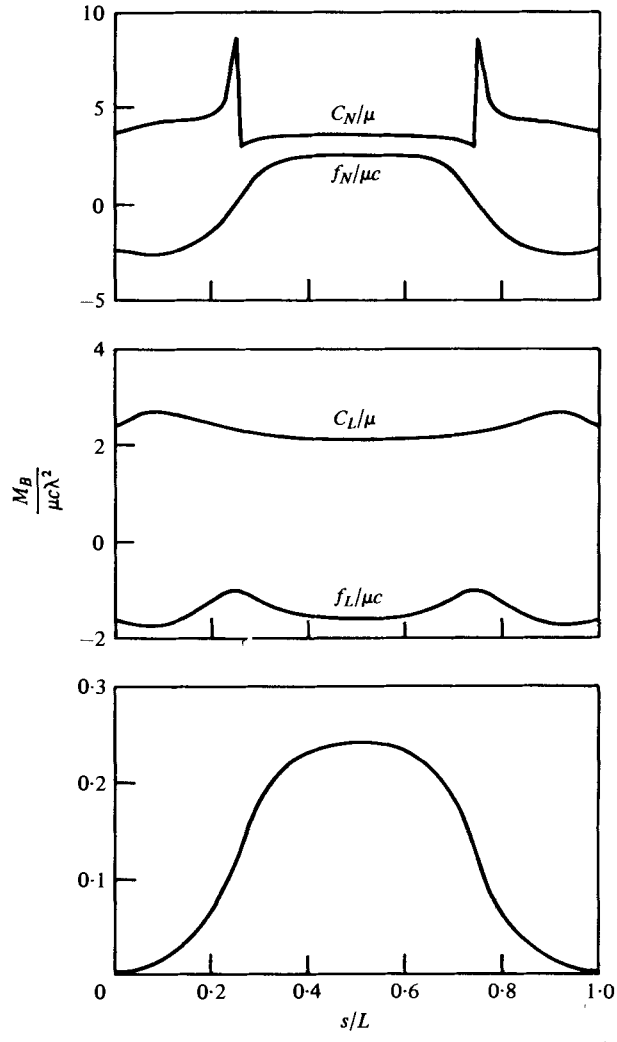

FIGURE 4. Spacial variation of f_N, f_L, C_N, C_L and M_B for a headless flagellum of shape given by $y = b \sin kx$ with $bk = 1$, $n = 1$ and $a/L = 0{\cdot}01$.

where the over-bar denotes cycle-averages (see, e.g. Pironneau & Katz 1974; Lighthill 1975). An additional propulsive parameter is

$$\kappa = \mu f L^2 |\bar{U}_{pX}| / \bar{E}, \tag{4.1b}$$

which can be interpreted as the straight-line distance travelled in the fixed co-ordinate system per unit of mechanical energy expended.

Sinusoidal wave forms

The time-varying values of selected propulsive quantities for the archetypal wave form are shown in figure 3. In the fixed system the translational velocities are periodic with the wave form but asymmetric in form. The change in sign of U_{pX} indicates that during part of the cycle the origin of the moving co-ordinate system moves in the same

direction as the travelling wave. (Quantities written without non-dimensionalization refer to the generic quantity.) In general the temporal variations of the three components of velocity in the moving co-ordinate system are similar to those derived using zeroth-order small amplitude theory (Pironneau & Katz 1974). However, U_{py} displays a moderately small asymmetry, not present at zeroth-order, which is due to the far-field contribution. The non-zero value of $\overline{U}_{pY}$ results in a moderate bias in the translation of the organism in a direction transverse to its 'propulsive axis'. Thus the total translational propulsive speed is actually given by $(\overline{U}_{pX}^2 + \overline{U}_{pY}^2)^{\frac{1}{2}}$. However, for sinusoidal wave forms the difference in value between this expression and $\overline{U}_{pX}$ was at worst equal to 6 % (for a flagellum with approximately one wavelength), and in most cases was less than 2 %. For the more accurate wave forms considered below, in all cases the difference was less than 1 % owing to minimal pitching. The power output varies in phase with U_{px} with a peak-to-peak variation equal to 128 % of the mean value ($\overline{E}/\mu c^2\lambda = 1{\cdot}47$).

The force distribution on the tail, effective resistance coefficients, and bending moment on the tail for the archetypal wave form at $t = 0$ are shown in figure 4. These plots are representative of the spatial variation of these quantities throughout the beat cycle. The normal component of force is approximately $+90°$ out of phase with the wave-form, although the variation of f_N is only approximately sinusoidal in shape. It has a period equal to that of the wave form, and changes sign during the second half of the cycle. The longitudinal force per unit length is relatively constant throughout the beat cycle, and is periodic with half the period of the sine wave form. The normal and longitudinal effective resistance coefficients are both fairly constant in space and time. The spikes in C'_N generally occur at points on the tail where the normal absolute velocity is very small (usually at extrema of the wave form). The spatial averages of $\overline{C}_N/\mu$, $\overline{C}_L/\mu$, and their ratio $\overline{C'_N/C'_L}$, are 3·62, 2·44, and 1·52 respectively. This ratio lies midway between the zeroth-order ratio, 1·41 [equation (2.14)] and 1·70 obtained from Lighthill's (1976) improved coefficients with $\delta/\Lambda = 0{\cdot}08937$ (see § 5). The bending moment, also shown in figure 4, displays a temporal variation similar to f_N. The spatial and temporal variations of the force per unit length, effective resistance coefficients, and bending moment for $n = 1{\cdot}5$ ($bk = 1$ and $a/L = 0{\cdot}01$) all exhibit the same qualitative behaviour as for the $n = 1$ case.

The number of wavelengths on a sinusoidal wave form with $bk = 1$ and $a/L = 0{\cdot}01$ was varied from 0·75 to 2·0. Flagella both with and without an attached head ($a_H/L = \frac{1}{36}$) were considered. When the phase speed is used for scaling purposes an increase in the number of wavelengths represents the change due to an addition to the length of the tail, since the wavelength and amplitude are fixed. If the combination fL is used to non-dimensionalize the velocity, all tail lengths are the same; an addition to the number of wavelengths pushes the peaks of the sinusoid closer together while simultaneously decreasing the amplitude, bk remaining unchanged. The non-dimensionalization involving the tail length is most appropriate in considering the effect of the variation of a wave-form parameter on an individual organism. For example, if it is of interest to determine the number of wavelengths at which a *particular* organism (L = constant) attains its maximum propulsive velocity, then the proper velocity scale is fL since λ varies as n changes.

Figure 5 shows the variation of $\overline{U}_{px}$ with n, the number of wavelengths. (Since the cycle average of $\overline{U}_{py}$ is always zero when the frequency is constant, it is not shown.)

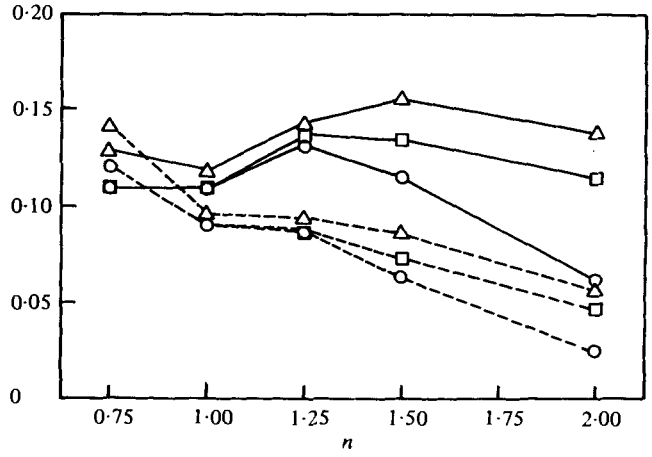

FIGURE 5. Time-averaged x component of propulsive velocity ($\bar{U}_{px}$) in the mean system as a function of the number of wavelengths for a flagellum with a head, with a non-interacting head and without a head. The shape is given by $y = b \sin k(x - ct)$ with $bk = 1$ and $a/L = 0{\cdot}01$. ——, $\bar{U}_{px}/c$; – – –, $\bar{U}_{px}/fL$. △, no head; ○, head; □, non-interacting head.

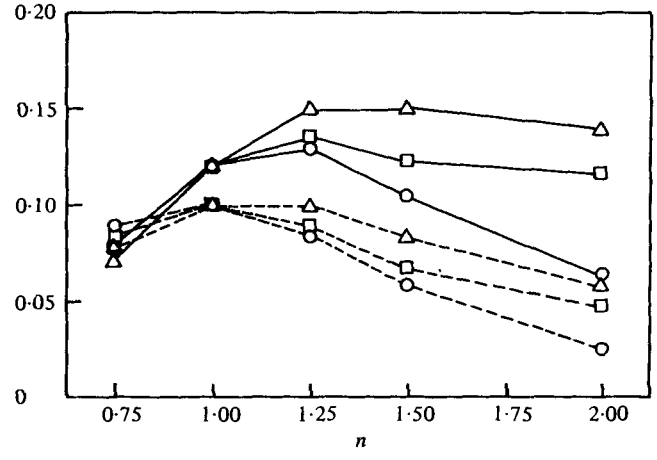

FIGURE 6. Time averaged X-component of propulsive velocity ($\bar{U}_{pX}$) in the fixed system as a function of the number of wavelengths for a flagellum with a head, with a non-interacting head and without a head. The shape is given by $y = b \sin k(x - ct)$ with $bk = 1$ and $a/L = 0{\cdot}01$. ——, $\bar{U}_{pX}/c$; – – –, $\bar{U}_{pX}/c$. Symbols as in figure 5.

It appears that, at least in the moving system, certain wavelengths are favoured. This is especially apparent in the plot of $\bar{U}_{px}/c$ where for the headless flagellum $n = 1{\cdot}5$ appears to represent a local maximum, while $n = 1$ and $n = 2$ are local minima. (In the figures, the absolute value of the velocity components is shown.) It is assumed that $n = 2$ approximates a minimum since as n approaches infinity, the pitching effect rapidly diminishes and $\bar{U}_{px}/c$ must rise to its limiting value of 0·180 (table 1).

The velocities in the fixed reference frame are displayed in figure 6. Here again the variation in $\bar{U}_{pX}$ shows marked maxima at particular wavelengths. However, within this range of n there is only a single preferred value – in the region between 1·0 and

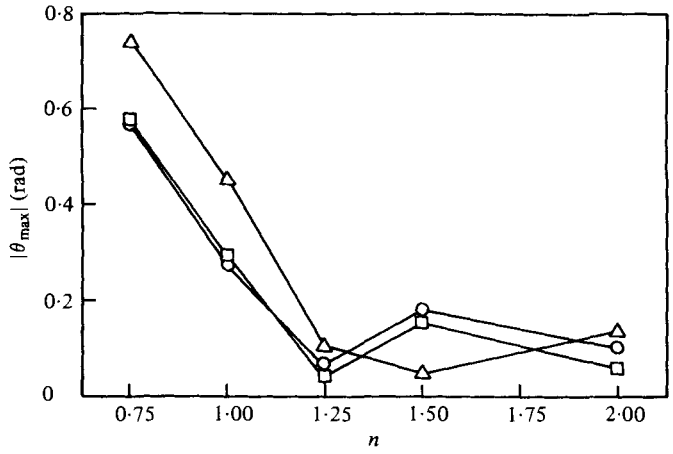

FIGURE 7. Absolute value of the maximum pitching angle (θ_{max}) as a function of the number of the wavelengths for a flagellum, with a head, with a non-interacting head and without a head. The shape is given by $y = b \sin k(x-ct)$ with $bk = 1$ and $a/L = 0{\cdot}01$. Symbols as in figure 5.

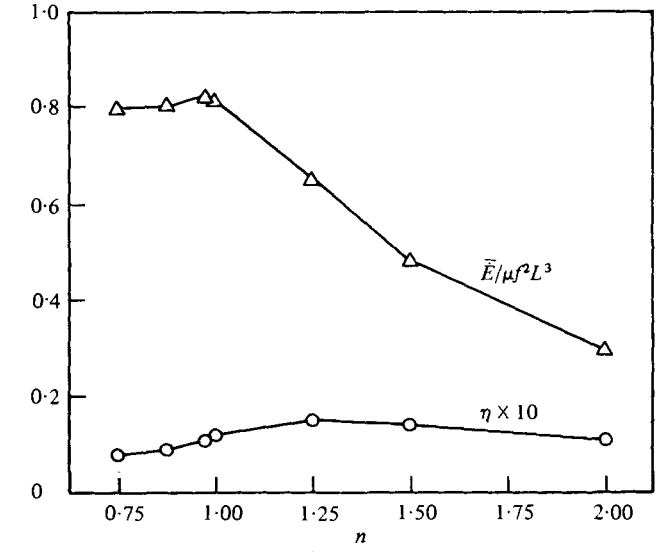

FIGURE 8. Time-averaged power output ($\bar{E}$) and propulsive efficiency (η) as functions of the number of wavelengths for a headless flagellum of shape given by $y = b \sin k(x-ct)$ with $bk = 1$ and $a/L = 0{\cdot}01$.

1·5 wavelengths for a headless flagellum. The reason for this is made evident in figure 7 which is a plot of $|\theta_{max}|$ versus n. This quantity indicates the relative effect of pitching on the translational velocities in the local co-ordinate system. The large value of $\bar{U}_{px}$ at $n = 0{\cdot}75$ is mitigated by the correspondingly high value of $|\theta_{max}|$. Conversely, the maximum in $\bar{U}_{px}$ at $n = 1{\cdot}5$ is essentially unchanged in the fixed system, since at that point $|\theta_{max}|$ is quite small. The variation in $\bar{U}_{pY}$ (not shown) also displays a marked variation with n and, within the range $n = 0{\cdot}75$ to $n = 2{\cdot}0$, a maximum occurs close to $n = 0{\cdot}9$ ($U_{pY}/c = 0{\cdot}029$). The bias in U_{pY} is caused by the small temporal asymmetry

in U_{pY} (introduced by the far-field contribution) which manifests itself in the fixed reference system. Thus it appears that if the object of a flagellum (with $bk = 1$, no head, and $a/L = 0{\cdot}01$) is to traverse a given straight line in the minimum time, it should deform its wave form into approximately 1·0 to 1·5 wavelengths, all other quantities notwithstanding.

Figure 8 shows the variation of both the power output and propulsive efficiency with the number of wavelengths for a headless flagellum. The power output exhibits a maximum at approximately $n = 1$ which is probably related to the coincident maximum in $\overline{U}_{pY}$. Rather than the power output alone, a more appropriate measure of the hydrodynamically optimum number of wavelengths is given by the propulsive efficiency η. This quantity shows a maximum at $n = 1{\cdot}25$. Both the non-dimensional power, of the form $\dot{E}/\mu c^2\lambda$ and the parameter κ [equation (4.1*b*)] increase monotomically with increasing n.

The effect of varying the number of wavelengths on a flagellum with an interacting head or with a non-interacting head is also shown in figures 5–7. In the latter case, the equilibrium conditions are modified as in § 2, but the far-field mutual velocity interaction between the tail and head is not included. The results for the x component of propulsive velocity (figure 5) are qualitatively similar to what might be expected, in light of the head analysis discussed in § 3. That is, the effect of a non-interacting head is generally to reduce the propulsive velocity of the body, though not as drastically as an interacting head does. An interesting phenomenon occurs between $n = 1$ and $n = 1{\cdot}25$, where the body with a head takes on velocity almost equal to that of the headless flagellum. The significance of this result is made evident in figure 6. In the fixed system, the flagellum with a head has a higher propulsive velocity than the headless body up to approximately 1·0 wavelengths. At this point, the curves for $\overline{U}_{pX}$ cross, and headless body swims faster. The reason for this curious behaviour can be seen in figure 7. Between $n = 0{\cdot}75$ and approximately $n = 1{\cdot}25$, the headless flagellum pitches significantly more than those with heads. Thus, even though the velocity in the moving co-ordinate system may be smaller for the body with a head, the velocity in the fixed reference frame can be larger owing to more moderate pitching. For values greater than $n = 1{\cdot}0$, the reduced pitching no longer compensates for head drag, and the headless flagellum has a higher velocity. The presence of a head can be thought of as producing two competing effects: reduced pitching at small values of wavelength, and increased drag.

Since the difference between the curves in figure 6 may lie within the error associated with the head model (see § 3) calculations for a flagellum with a head of intermediate radius ($a_H/L = \frac{1}{72}$) were made. These results also indicated a crossover in propulsive velocity, but the point was shifted slightly to the right. Therefore, it does not appear as if this phenomenon is artifactual. An additional point of interest is that while the headless flagellum exhibits a maximum in power output at approximately $n = 1$, the power outputs of the flagella with a head decline monotonically with $n (n \geqslant 0{\cdot}75)$.

The effect of varying the amplitude–wavelength ratio bk ($= 2\pi b/\lambda$) between 0·1 and 1·5 was investigated for a headless, sinusoidal travelling wave with $n = 1$ and $a/L = 0{\cdot}01$. The variation of $\overline{U}_{pX}$, shown in figure 9, exhibits the sigmoid shaped variation also found by Hancock (1953) and Pirroneau & Katz (1974). The maximum pitching angle also increases monotonically with bk as does the power output. In figure 10 the propulsive efficiency displays a maximum in the region of $bk = 1{\cdot}25$, well

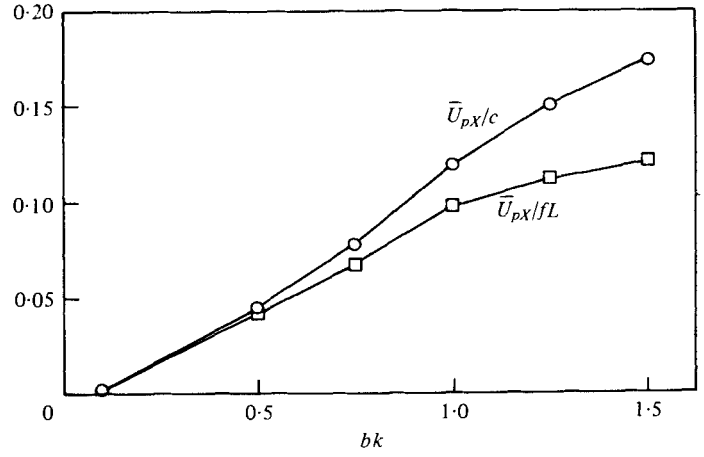

FIGURE 9. Time-averaged X component of velocity ($\bar{U}_{pX}$) in the fixed system as a function of bk for a headless flagellum of shape given by $y = b \sin k(x - ct)$ and containing one wavelength ($n = 1$) with $a/L = 0{\cdot}01$.

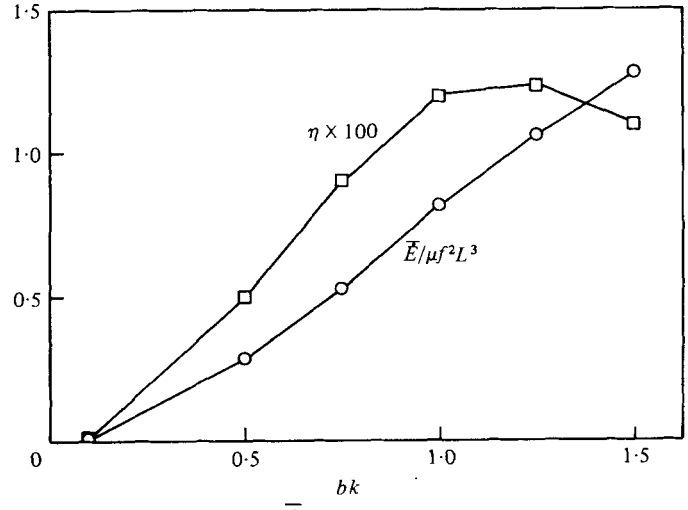

FIGURE 10. Time-averaged power output ($\bar{E}$) and propulsive efficiency (η) as a function of bk for a headless flagellum of shape given by $y = b \sin k(x - ct)$ and containing one wavelength ($n = 1$) with $a/L = 0{\cdot}01$.

within the physiological range. The power output, also shown in figure 10, increases monotonically with bk. The results for $n = 2$ (not shown) are qualitatively similar to those for one wavelength.

To estimate the effect of the radius ratio the representative archetypal wave form ($bk = 1$, $n = 1$, no head) was chosen for study. The results for three values of radii are shown in table 2. A 100 % increase in a/L, from 0·01 to 0·02, decreases $\bar{U}_{pX}$ by 17 %, increases the power output by 13 %, and decreases the efficiency by approximately 36 %. If the radius ratio is decreased by 50 %, $\bar{U}_{pX}$ increases by 5 %. $\bar{E}$ decreases by 24 %, and the efficiency increases by 55 %. The change in magnitude of $\bar{U}_{pX}$ between $a/L = 0{\cdot}01$ and 0·02 for a one wavelength flagellum is about twice as great as was

Radius (a/L)	$\bar{U}_{pX}/fL$	$\bar{U}_{pY}/fL$	$\lvert\theta_{max}\rvert$	$\bar{E}/\mu f^2L^3$	$\mu L\bar{U}_{pX}^2/\bar{E}$
0·005	−0·103	0·025	0·478	0·623	0·017
0·01	−0·098	0·023	0·450	0·818	0·011
0·02	−0·081	0·021	0·494	0·928	0·007

TABLE 2. Radius variation

found for a change from $a/\lambda = 0{\cdot}01$ to $a/\lambda = 0{\cdot}02$ for the infinite flagellum (see § 3). The velocity decreases with increasing a/L because the ratio C_N/C_L is reduced; however, the power output increases because the absolute values of the resistance coefficients are increased. The reverse occurs for a decrease in the radius.

Wave forms given by $\alpha(s,t)$

For non-periodic wave-form shapes of physiological interest, the representation given by (2.7) is used. Here the natural length scale is L rather than λ. Similarly, the phase speed, as measured along the curved flagellum, q or the beat frequency f are used to scale quantities involving the time dimension, rather than c. We have chosen the expression

$$\alpha(s,t) = \alpha_0\sigma(s)\cos 2\pi[s/\Lambda(s) - f(s)\,t] \tag{4.2}$$

to generate the wave forms in this subsection.

Before considering these cases, it is desirable to link the preceding parametric studies, based on a sinusoidal wave form in x, with the variable amplitude and wavelength studies which follow. The equation $\alpha(s,t) = \alpha_0\cos 2\pi(s/\Lambda - ft)$ produces a good approximation to a sine wave in the x, y plane for $bk \lesssim 1$. Specifically, for $\alpha_0 = 51°$ an equivalent bk of 1·003 is found, and for $\alpha_0 = 45°$ (the maximum slope angle of a sinusoidal wave form with $bk = 1$) the resulting curve has a bk equivalent to 0·861. (For $\alpha_0 = 51°$, the average deviation between the two curves is 3·8 % of the maximum amplitude of the sine wave; the maximum deviation is 7·2 %.) When this expression for α is inserted into the model, with these two values of α_0, results are obtained which bracket those found for the archetypal sinusoidal wave form considered previously. For example the archetypal value for $\bar{U}_{pX}/fL$ is −0·098. This compares with values of −0·102 for $\alpha_0 = 51°$ and −0·089 for $\alpha_0 = 45°$.

Spermatozoa of several mammalian species, under certain circumstances, produce waveforms exhibiting an amplitude envelope with grows with distance from the head–tail junction (e.g., human, Katz, Mills & Pritchett 1978; bull, Rikmenspoel 1965; ram, Denehy 1975; guinea pig and hamster, Katz, Yanagimachi & Dresdner 1978.) To model this behaviour analytically, and to evaluate the resulting propulsive motion, we have employed (4.2) with Λ and f constant, $s \in [0, \Lambda = L]$, and $\sigma(s) = \beta^s$. The maximum slope angle at $s = 0$ (i.e. α_0) was chosen to be 5·1°, and the maximum amplitudes (at $s = L$) were 0·5, 1 and 1·5 times the peak amplitude of the constant-amplitude wave form generated with $\alpha_0 = 51°$. Thus, β takes on the values 5, 10 and 15, respectively. Composite plots of the resulting wave-form shapes, at four representative times, are shown in figure 11. Figure 12 displays the results for these wave forms with a head $(a_H/L = \frac{1}{36})$. The values for $\bar{U}_{pX}$ are substantially less than that of the $\alpha_0 = 51°$ constant

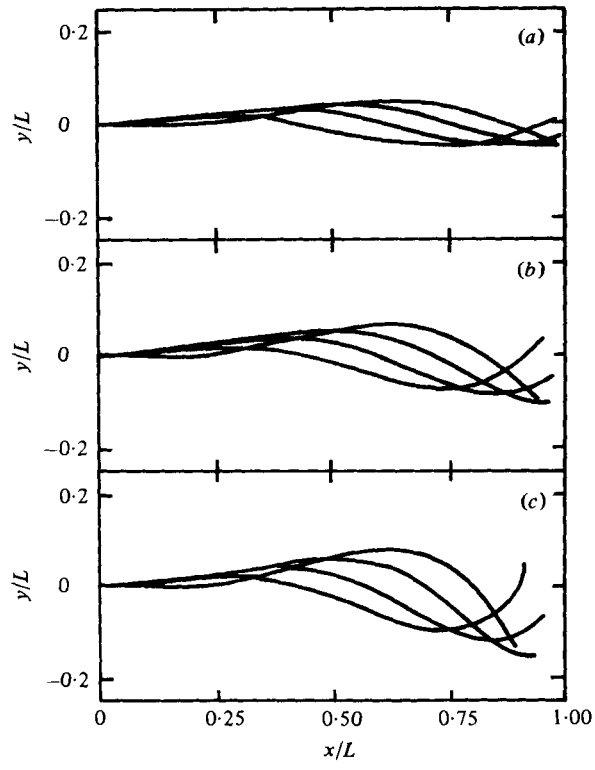

FIGURE 11. Wave forms with variable amplitude. (a) $\beta = 5$; (b) $\beta = 10$; (c) $\beta = 15$.

amplitude wave form ($-0{\cdot}102$). Even with $\beta = 15$, the velocity is less than a third of this comparative value. (It is roughly equivalent to a sinusoid with $bk = 0{\cdot}5$, see figure 9.) The total power output shows a similar reduction in level, as does the propulsive efficiency. The magnitude of $\bar{U}_{pY}/fL$ is less than or equal to 0·02 in all cases.

In addition to variable amplitude, flagellated organisms may also exhibit variable wavelength. [Human sperm in seminal plasma (Mills 1978) and cervical mucus (Katz, Mills & Pritchett 1978) exhibit both these properties.] Since $q = \Lambda f$, in general, if $\Lambda = \Lambda(s)$ then either q or f can be constant while the other parameter varies along the flagellum. Each of these specifications, constant phase speed or constant frequency, results in a different expression for $\alpha(s,t)$ and, therefore a distinctive beat pattern. From (4.2) the constant frequency wave forms are generated by

$$\alpha = \alpha_0 \sigma(s) \cos 2\pi[s/\Lambda(s) - ft] \tag{4.3}$$

and the constant phase speed wave forms by

$$\alpha = \alpha_0 \sigma(s) \cos 2\pi[(s - qt)/\Lambda(s)]. \tag{4.4}$$

Before a comparison of the propulsive characteristics of these two representations can be made, the 'frequency' of the beat cycle in the case of constant phase speed must be examined. In this case, since each tail point can have a unique period of oscillation, a single beat frequency may be undefinable. However, a special set of circumstances can be assumed in order to avoid this situation. The wavelength is made to change

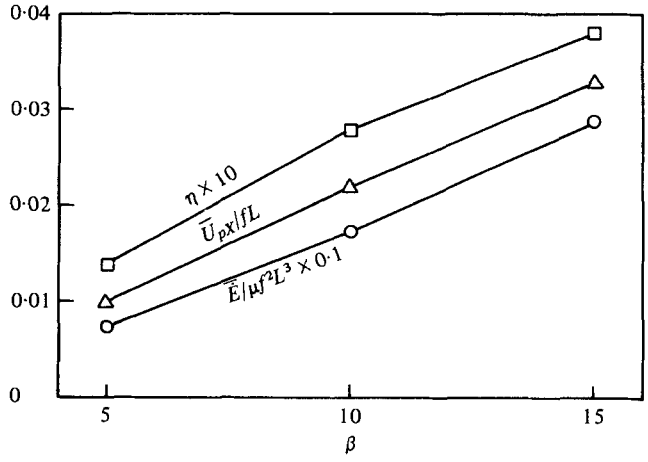

FIGURE 12. Time-averaged fixed system X-component of propulsive velocity ($\bar{U}_{pX}$), power output ($\bar{E}$) and propulsive efficiency (η) as functions of β for the wave forms shown in figure 11.

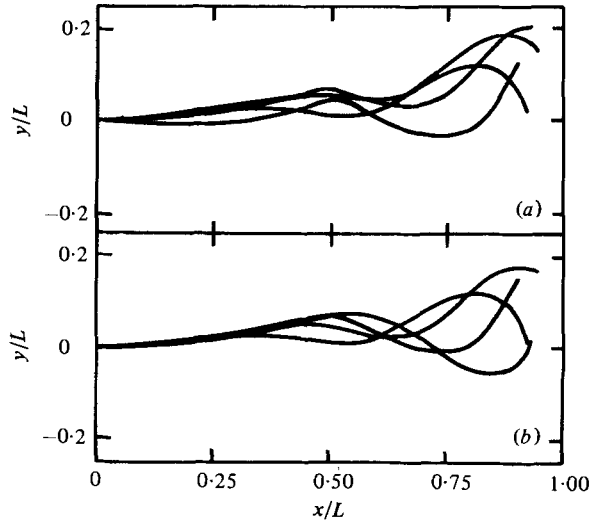

FIGURE 13. Wave forms with variable amplitude and wavelength at four representative time instants. (*a*) Constant frequency; (*b*) constant phase speed.

rapidly from one constant value ($\Lambda/L = \frac{4}{3}$) to another ($\Lambda/L = \frac{2}{3}$) at the midpoint $s/L = 0{\cdot}5$. Thus the frequency of the first portion of the tail is half that of the second portion. The change-over must encompass an extremely small region, since the points in the transition zone which have not returned to their original position after the beat period, will adversely affect the position of points distal to themselves through (A 4). The functions $\sigma(s)$ and $\Lambda(s)$ were taken as

$$\alpha_0\sigma(s) = 5{\cdot}1°(15)^s, \quad \Lambda(s) = 1 - 0{\cdot}2125\tan^{-1}[1000(s-0{\cdot}5)]. \tag{4.5}$$

Figure 13 shows the constant frequency and constant phase speed wave forms, at four representative times. At several times instants the transition point is clearly visible.

Case	$\bar{U}_{pX}/fL$	$\bar{U}_{pX}/q$	$\bar{U}_{pX}/f_A L$	$\lvert\theta_{max}\rvert$	$\dot{E}/\mu f^2 L^3$	$\dot{E}/\mu q^2 L$	$\dot{E}/\mu f_A^2 L^3$	$\mu L \bar{U}_{pX}^2/\dot{E}$
Constant frequency	−0·020	N.A.	−0·020	0·261	0·125	N.A.	0·125	0·0032
Constant phase speed	N.A.	−0·037	−0·037	0·287	N.A.	0·368	0·368	0·0037

N.A. = not applicable.

TABLE 3. Variable amplitude and wavelength wave forms, f_A = average frequency.

For the constant frequency case the natural scaling parameters are μ, L and q. For the constant phase speed formulation an average frequency can be defined for purposes of comparison.

The results for these two cases are shown in table 3. By any means of comparison, the constant phase speed wave form swims roughly twice as fast as that with constant frequency. The power output is also several times larger for the constant phase speed case. The propulsive efficiency indicates a moderate advantage for the constant phase speed case. The maximum pitching angle is approximately the same in both cases. The values for $\bar{U}_{pY}$ (not tabulated) are all 10 % or less of the corresponding $\bar{U}_{pX}$ value.

General discussion of results

When the number of wavelengths on the sinusoidal wave form is varied, it has been found that certain values of n are less advantageous to forward propulsive movement than others. In the fixed reference system, values of wavelengths in the vicinity of 1·0 and 1·5 appear preferable. The propulsive efficiency also shows a maximum in this region. (As figure 10 indicates a bk in the region of 1·25 is optimum, at least for $n = 1$.) Since the movement characteristics of many uniflagellar micro-organisms, with reasonably small heads and $bk \simeq 1$, fall within this region of n (Brennen & Winet 1977), it is tempting to conclude that this phenomenon is the result of an attempt to optimize propulsive movements. Such teleological speculation should be tempered by the fact that the wave form of a flagellated organism is determined by numerous physiological, morphological and environmental factors, only a few of which have been included in the present study.

It was also found that up to approximately $n = 1{\cdot}0$, a body with a head has a larger average forward propulsive velocity than the headless flagellum. This interesting phenomenon can be attributed to the effect of the head in reducing pitching within this range of wavelengths. However, one must bear in mind that the interactive effect of the head is only approximately modelled, and the analytic sinusoidal wave form is representative and not descriptive. Consequently, the absolute values associated with the differences between the body with and without a head, and the location of the cross-over point, are only indicative. The principal conclusions to be drawn are that depending upon the situation, the cell body can either reduce or augment the forward propulsive velocity, and that the complete equilibrium conditions must be applied in order to realize this effect. It should be noted, however, that the presence of a head does not uniformly diminish pitching. Figure 7 shows that for $n = 1{\cdot}5$ the headless flagellum actually pitches less. This illustrates the fact that the head modifies the equilibrium matrix (2.22) in a manner which allows for a greater range of possible values of Ω.

Case	$\bar{U}_{pX}/fL$	$\bar{U}_{pY}/fL$	$\lvert\theta_{max}\rvert$	$\bar{E}/\mu f^2L^3$	$\mu L\bar{U}_{pX}^2/\bar{E}$
Present theory, no head	−0·098	0·023	0·450	0·818	0·012
Unidirectional propulsion, no head	−0·137	0	0	0·982	0·019
Present theory, head	−0·100	0·012	0·271	1·132	0·009
Unidirectional propulsion, head	−0·123	0	0	1·163	0·103

TABLE 4. Unidirectional propulsion ($bk = 1$, $n = 1$, $a/L = 0{\cdot}01$, $a_H/L = \frac{1}{36}$).

Case	$\bar{U}_{pX}/fL$	$\bar{U}_{pY}/fL$	$\lvert\theta_{max}\rvert$	$\bar{E}/\mu f^2L^3$
Present theory, $n = 0{\cdot}5$	−0·049	0·000	0·638	0·570
Lighthill, $n = 0{\cdot}5$	−0·061	0·000	0·633	0·525
Present theory, $n = 1{\cdot}0$	−0·098	0·023	0·450	0·818
Lighthill, $n = 1{\cdot}0$	−0·11[illegible]	0·026	0·472	0·771
Present theory, $n = 1{\cdot}5$	−0·083	0·000	0·048	0·483
Lighthill, $n = 1{\cdot}5$	−0·091	0·000	0·028	0·453

TABLE 5. Comparison with Lighthill's (1976) theory ($bk = 1$, $a/L = 0{\cdot}01$).

Finally it is important to emphasize the significant differences between the two variable wavelength cases. For the analytic shapes shown in figure 13 the constant phase speed flagellum has roughly twice the average forward propulsive velocity of the constant frequency wave form. Thus, great care should be taken both in the hydrodynamic modelling of actual flagellar beat shapes, and in the acquisition and interpretation of experimental data.

5. Comparison with other results

Several alternative theories and problem specifications are available for comparison and evaluation of the results presented in this work. In § 3, comparison was made with Hancock (1953) and Shen *et al.* (1975) for the large amplitude sinusoidal wave form of infinite length; here only finite flagella are considered.

If the propulsive motion of an organism is assumed to be unidirectional, the analysis is somewhat simplified. Table 4 shows the effect of this simplification on the complete theory for selected movement characteristics. It is seen that when the influence of pitching and transverse propulsive motion is neglected, the propulsive velocity is overestimated by about 40 % for the headless flagellum with a sinusoidal travelling wave form, $bk = 1$, $n = 1$ and $a/L = 0{\cdot}01$ (23 % with a head, $a_H/L = \frac{1}{36}$). Concomitantly, the power output is also increased by 20 % without a head and 3 % with a head. The propulsive efficiencies are all overestimated by like amounts.

Recently, Lighthill (1976) has developed resistance coefficients which more accurately account for the far-field contribution than the original Gray & Hancock (1955) expressions. These improved coefficients are

$$C_N = 4\pi\mu/[\ln(2\delta/a) + 0{\cdot}5], \quad C_L = 2\pi\mu/\ln(2\delta/a). \tag{5.1}$$

Note that this is the same set of expressions given in (2.14) except for 0·5 in C_L. As noted previously, Lighthill also suggested that δ/Λ be assigned the value of 0·08937.

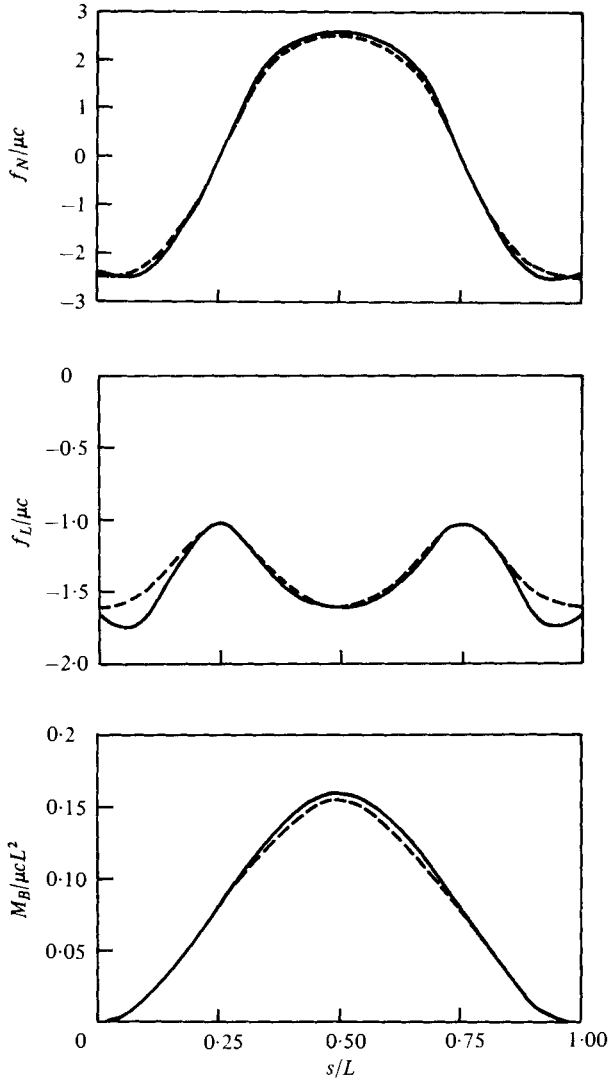

FIGURE 14. Spacial variation of f_N, f_L and M_B for a headless flagellum of shape given by $y = b \sin kx$ with $bk = 1$, $n = 1$, and $a/L = 0{\cdot}01$. ——, present theory; – – –, zeroth-order theory with resistance coefficients of Lighthill (1976).

A comparison between the zeroth-order solution based on (5·1) and the full iterative procedure has been carried out on a sinusoidal waveform with $bk = 1$, $a/L = 0{\cdot}01$, and three values for the number of wavelengths. Generally, as seen in table 5, the use of the Lighthill coefficients somewhat overestimates the values of $\overline{U}_{pX}$ and $\overline{U}_{pY}$, and underestimates $\overline{E}$. A similar comparison for the variable amplitude s-generated wave form discussed in § 4 with $\beta = 15$ was also carried out with qualitatively very similar results. For example, with the improved resistance coefficients, $\overline{U}_{pX}$ is approximately 14 % higher for the headless flagellum and 6 % higher for a body with a head. Figure 14 shows the spatial variations in the normal and tangential force per unit length and the bending moment on the tail for the sinusoid with $n = 1$. The agreement with the

iterative solution is remarkably close in all cases. On the basis of this preliminary comparison, it appears that the coefficients introduced by Lighthill offer a simple and fairly accurate means of estimating the propulsive motion of an isolated, slender micro-organism.

Pironneau & Katz (1974) examined the motion of an unconstrained, large amplitude sawtoothed wave form with an analysis based upon the resistance coefficients given by (2.14). Qualitatively, these results are very similar to those found in the present study. Their curves for $\overline{U}_{pX}$, $\overline{E}$, and $\mu L\overline{U}_{pX}^2/\overline{E}$ as functions of bk illustrate the same general trends as shown in figures 9 and 10.

More recently Johnson (1977) has developed a theory and technique for determining the Stokes flow past slender bodies in general motion. Basically, the method involves the solution, by an expansion technique, of an integral equation similar to (2.3). Local curvature effects are accounted for by the inclusion of higher-order viscous singularities such as rotlets and stresslets. In § 3 a comparison between Johnson's theory and the present study for a torus was examined. The results showed quite good agreement between the two methods (within 5 %). Johnson also considered the unidirectional translation of flagellar-like wave forms representative of the spermatozoa of two invertebrate species. Since the equilibrium conditions were not imposed, the single component of $\mathbf{U}_p$ was specified rather than determined simultaneously with the force per unit length on the body. The propulsive velocity of a self-propelling organism can be determined by treating this quantity as an independent parameter and determining the value at which the total force on the body is zero. The approximate effect of a spherical head on the flagellar motion is also included in Johnson's model. His method of analysis is somewhat more rigorous than the head procedure employed here and, therefore, may be more accurate. Johnson found that the average thrust produced by the flagellum (indicative of the propulsive velocity) for a headless body showed 'favourable' regions as a function of the number of wavelengths. The pattern is similar to that shown in figures 5 and 6, and discussed in § 4. Qualitative differences between the two techniques may be due, in part, to the fact that U_{py} and Ω are taken as identically zero in Johnson's analysis. In addition, there are dissimilarities in the wave-form shapes. When compared to the experimentally determined propulsive velocities of the self-propelling spermatozoa modelled by Johnson, his theory overestimated these values. In addition to the various possible reasons for this discrepancy given by Johnson (all of which seem reasonable), a substantial portion of the overestimation may have been due to not having applied the full system of equilibrium equations (see above). This would especially seem likely if the sperm pitched considerably. Also, as pointed out by Johnson, the analytic wave form did not accurately model the spermatozoa's shape near the proximal end of the flagellum. If the amplitude in this region of the actual spermatozoa were reduced, owing in part perhaps, to the presence of a head, the resulting propulsive velocity of the organism might be significantly decreased (see § 4).

Of course, the ultimate test of any new theory or method is comparison to pertinent experimental results. At this time, unfortunately, no adequate information on the detailed movements of a flagellated organism is available. For this reason, only representative, analytic wave forms have been used. The extremely difficult problems in acquiring data on the time-varying shape and velocity distributions along the tail length are discussed extensively in Mills (1978). The time-averaged propulsive

velocities of numerous micro-organisms have been compiled by various researchers and the results presented herein lie well within the wide variation they exhibit (see, e.g., the extensive tabulation in Brennen & Winet 1977; Overstreet & Katz 1977).

6. Concluding remarks

Our primary purpose has been to develop an accurate and practical method for mathematically modelling the fluid mechanical behaviour of motile, uniflagellar micro-organisms. The method has been systematically used to investigate the propulsive movement characteristics of a variety of representative beat shapes. Several future applications and extensions are foreseeable. These include the determination of the flow field about the organism, allowance for axial taper, and consideration of general three-dimensional beat shapes (or special cases, such as circular helices). A largely unexplored area, to which the iterative procedure might be profitably applied, is the fluid mechanics of non-isolated flagellates.

This work was partially supported by the National Institutes of Health, grant HD 8018 and the World Health Organization, contract 75179. One of us (R. D. D.) acknowledges the support of an NIH Biomedical Engineering Traineeship.

Appendix. Co-ordinate systems and wave-form representations

In previous studies of the fluid mechanics of self-propelling slender bodies, several representations for the moving co-ordinate system have been developed. The first system was introduced by Taylor (1951). Among its advantages is that in this system an analytic expression for the beat velocity of a sinusoid can be easily derived in terms of an elliptic integral. Its major drawback, however, is its inapplicability to move general travelling wave forms. This system will not be reviewed here. Wave forms of the type $y = y(x, t)$ can be analysed by using a method introduced by Keller & Rubinow (1976). They applied it only to sinusoids, in which case analytic expressions for the beat velocity can be derived, but it is easily extended to more general flagellar shapes. A third representation, used by Brokaw (1970) and Shack *et al.* (1974) will be referred to as the head co-ordinate system. It is adaptable to a wide variety of wave forms, but necessitates numerical computations for the beat velocity.

We first consider planar wave forms given by $y = y(x, t)$. In this case the x co-ordinate of a point on the tail is related to the s co-ordinate along the body centre-line by the integral

$$s[x(t), t] = \int_0^{x(t)} \left[1 + \left(\frac{dy}{dx'}\right)^2\right]^{\frac{1}{2}} dx'. \tag{A 1}$$

Differentiating (A 1) with respect to t, and noting that $ds/dt = 0$ for an inextensible flagellum, gives

$$\frac{dx}{dt} = -\frac{\int_0^{x(t)} \frac{\partial}{\partial t}\left[1 + \left(\frac{dy}{dx'}\right)^2\right]^{\frac{1}{2}} dx'}{\left[1 + \left(\frac{dy}{dx}\right)^2\right]^{\frac{1}{2}}}. \tag{A 2}$$

For the special case of a sinusoid the integral in (A 2) can be evaluated analytically. In this case the beat velocities are given by

$$\hat{u}_x = c - c[(1 + b^2k^2\cos^2 ckt)/1 + b^2k^2\cos^2 k(x-ct)]^{\frac{1}{2}}, \tag{A 3a}$$

$$\hat{u}_y = bk(c - \hat{u}_x)\cos k(x-ct). \tag{A 3b}$$

For more general wave forms (A 2) must be solved numerically.

In the head system, the wave form is defined by a travelling wave along s rather than x, and is given by $\alpha = \alpha(s,t)$. The position co-ordinates are described parametrically by the integrals

$$x(s,t) = \int_0^s \cos\alpha(s',t)\,ds', \quad y(s,t) = \int_0^s \sin\alpha(s',t)\,ds'. \tag{A 4}$$

Since this is a natural Lagrangian representation, the beat velocity is simply the time derivative of (A 4); therefore,

$$\hat{u}_x = -\int_0^s \sin\alpha(s',t)\frac{\partial\alpha}{\partial t}\,ds', \quad \hat{u}_y = \int_0^s \cos\alpha(s',t)\frac{\partial\alpha}{\partial t}\,ds'. \tag{A 5}$$

It can be seen that the head ($s = 0$) is always located at the point $(0, 0)$. Since the beat velocity of this point is identically zero, the total velocity of the head is interpreted as the propulsive velocity of the organism. This is not the situation for the propulsive velocity resulting from a mean system representation. Thus, instantaneous comparisons between propulsive velocities of the two systems cannot be made directly. However, since the velocity of the point $s = 0$ about the point $x = 0$, in the mean system, is periodic in time (for the case of periodic travelling waves), time-averaged quantities may be compared.

Note

Since the completion of this study, two papers have appeared which also present improved mathematical theories of the hydrodynamics of the propulsion of uniflagellar micro-organisms. In both cases the mathematical methodologies have many similarities to that of the present paper. However, the applications are different in that our emphasis is directed towards the movement of mammalian spermatozoa. Higdon (1979) has developed a fluid mechanical model and solution technique very similar to the present study. The primary difference is that Higdon includes the exact singularity system necessary to obtain the no-slip velocity boundary condition on a spherical cell body. He has conducted several parameter studies on sinusoidal wave forms (the only beat shapes considered), some of which are identical to those in this paper. Both qualitatively and quantitatively the results are quite close. For example, for a headless flagellum with $n = 1$ and $a/L = 0{\cdot}01$, the variation of $|\mathbf{U}_p|/c$ with bk appears to be within about 5 %, and the efficiency (which is defined slightly differently) peaks in the range $1 \lesssim bk \lesssim 1{\cdot}25$ for both studies. Although not specifically mentioned, it appears (from figure 12 in Higdon) that the organism translates with a small lateral bias. For a flagellum with $a_H/L = 1/36$ and $n = 1$, graphical interpretation of his data suggests a propulsive velocity slightly greater value than found by us. In looking at the accuracy of the Lighthill force coefficients, Higdon has also shown that their use somewhat overestimates the propulsive velocity and underestimates the power output.

In the second paper, Johnson & Brokaw (1979) have applied the slender body theory of Johnson (1977) to wave forms generated by a mathematical model of flagellar contraction (Brokaw 1972). These beat shapes have a relatively constant wavelength ($1{\cdot}33 \lesssim n \lesssim 2$) and a moderately increasing amplitude similar to some non-mammalian spermatozoa. The purpose of the paper was to test the accuracy of resistive force theory for such realistic wave forms. Johnson & Brokaw demonstrated that for a headless flagellum the Lighthill coefficients produce results indistinguishable from the more accurate theory, as was borne out in our study. The presence of a cell body ($a_H/L = \frac{1}{20}$) reduced the agreement somewhat. The temporal variation of C'_N and C'_L, shown in Johnson & Brokaw, is also quite similar to our results.

Since both Higdon and Johnson & Brokaw, when considering flagella with small cell bodies, obtained very similar results to the present study, it seems likely that the reduction in accuracy associated with our approximate head model does not significantly alter our results concerned with cell bodies of relatively small radii.

REFERENCES

Batchelor, G. K. 1970 Slender-body theory for particles of arbitrary cross section in Stokes flow. *J. Fluid Mech.* **44**, 419–440.

Blake, J. 1972 A model for the micro-structure in ciliated organisms. *J. Fluid Mech.* **25**, 1–23.

Brennen, C. & Winet, H. 1977 Fluid mechanics of propulsion by cilia and flagella. *Ann. Rev. Fluid Mech.* **9**, 339–398.

Brokaw, C. J. 1970 Bending moments in free-swimming flagella. *J. Exp. Biol.* **53**, 445–464.

Brokaw, C. J. 1972 Computer simulation of flagellar movement. I. Demonstration of stable bend propagation and bend initiation by the sliding filament model. *Biophys. J.* **12**, 564–586.

Chwang, A. T. & Wu, T. Y. 1971 A note on the helical movement of micro-organisms. *Proc. Roy. Soc.* B **178**, 327–346.

Cox, R. G. 1970 The motion of long slender bodies in a viscous fluid, Part 1. General theory. *J. Fluid Mech.* **44**, 791–810.

Denehy, M. A. 1975 The propulsion of nonrotating ram and oyster spermatozoa. *Biol. Reprod.* **13**, 17–29.

Dresdner, R. 1978 Theoretical Studies on the motion of self-propelled flagella. Ph.D. thesis, University of California, Berkeley.

Garcia de la Torre, J. & Bloomfield, V. A. 1977 Hydrodynamic theory of swimming of flagellated micro-organisms. *Biophys. J.* **20**, 49–67.

Gray, J. & Hancock, G. J. 1955 The propulsion of sea-urchin spermatozoa. *J. Exp. Biol.* **32**, 802–814.

Hancock, G. J. 1953 The self-propulsion of microscopic organisms through liquids. *Proc. Roy. Soc.* A **217**, 96–121.

Happel, J. & Brenner, H. 1973 *Low Reynolds Number Hydrodynamics*, 2nd rev. edn. Leyden: Noordhoff.

Higdon, J. J. L. 1979 A hydrodynamic analysis of flagellar propulsion. *J. Fluid Mech.* **90**, 685–711.

Hildebrand, F. B. 1965 *Methods of Applied Mathematics*, 2nd edn. Englewood Cliffs, New Jersey: Prentice Hall.

Holwill, M. E. J. & Miles, C. A. 1971 Hydrodynamic analysis of non-uniform flagellar undulations. *J. Theor. Biol.* **31**, 25–42.

Johnson, R. E. 1977 Slender-body theory for Stokes flow and flagellar hydrodynamics. Ph.D. thesis, California Institute of Technology, Pasadena.

Johnson, R. E. & Brokaw, C. J. 1979 Flagellar hydrodynamics. A comparison between resistive-force theory and slender-body theory. *Biophys. J.* **25**, 113–127.

KATZ, D. F. & PEDROTTI, L. 1977 Geotaxis by motile spermatozoa: Hydrodynamic reorientation. *J. Theor. Biol.* **67**, 723–732.

KATZ, D. F., MILLS, R. N. & PRITCHETT, T. R. 1978 The movement of human spermatozoa in cervical mucus. *J. Reprod. Fert.* **53**, 259–265.

KATZ, D. F., YANAGIMACHI, R. & DRESDNER, R. D. 1978 Movement characteristics and power output of guinea-pig and hamster spermatozoa in relation to activation. *J. Reprod. Fert.* **52**, 167–172.

KELLER, J. B. & RUBINOW, S. I. 1976 Swimming of flagellated microorganisms. *Biophys. J.* **16**, 151–170.

LADYZHENSKAYA, O. A. 1969 *The Mathematical Theory of Viscous Incompressible Flow*, 2nd edn. Gordon and Breach.

LIGHTHILL, M. J. 1975 *Mathematical Biofluiddynamics.* Philadelphia: SIAM.

LIGHTHILL, M. J. 1976 Flagellar hydrodynamics. *SIAM Rev.* **18**, 161–230.

MESTRE, N. J. DE & KATZ, D. F. 1974 Stokes flow about a sphere attached to a slender body *J. Fluid Mech.* **64**, 817–826.

MILLS, R. 1978 Experimental Studies on the Hydrodynamics of Human Spermatozoa. Ph.D. thesis, University of California, Berkeley.

OVERSTREET, J. W. & KATZ, D. F. 1977 Sperm transport and selection in the female genital tract. In *Development in Mammals*, vol. 2 (ed. M. H. Johnson), pp. 31–65. North-Holland.

PIRONNEAU, O. & KATZ, D. F. 1974 Optimal swimming of flagellated micro-organisms. *J. Fluid Mech.* **66**, 391–415.

RIKMENSPOEL, R. 1965 The tail movement of bull spermatozoa. Observations and model calculations. *Biophys. J.* **5**, 366–392.

SHACK, W. J., FRAY, C. S. & LARDNER, T. J. 1974 Observations on the hydrodynamics and swimming motions of mammalian spermatozoa. *Bull. Math. Bio.* **36**, 555–565.

SHEN, J. S., TAM, P. Y., SHACK, W. J. & LARDNER, T. J. 1975 Large amplitude motion of self-propelling slender filaments at low Reynolds numbers. *J. Biomech.* **8**, 229–236.

TAYLOR, G. I. 1951 Analysis of the swimming of microscopic organisms. *Proc. Roy. Soc.* A **209**, 447–461.

TAYLOR, G. I. 1952 The action of waving cylindrical tails in propelling microscopic organisms. *Proc. Roy. Soc.* A **211**, 225–239.

TILLETT, J. P. K. 1970 Axial and transverse Stokes flow past slender axisymmetric bodies. *J. Fluid Mech.* **44**, 401–417.

TUCK, E. O. 1964 Some methods for flows past blunt slender bodies. *J. Fluid Mech.* **18**, 619–635.